Supplementary Information

Thermoresponsive Ionogels with Highly Switchable Adhesion Properties Based on Dynamic Interchain Interactions

Yen-Chun Chen[1], Ming-Xiang Zhang[1], Pin-Hao Lin[1], Li-Yu Lo[1], Pei-Ting Lin[1], Chia-Yu Cho[1] & Yao-Joe Yang[1,2]*

[1]Department of Mechanical Engineering, National Taiwan University, Taipei, Taiwan, ROC

[2]Graduate School of Advanced Technology, National Taiwan University, Taipei, Taiwan, ROC

*Corresponding authors: yjy@ntu.edu.tw

This file includes:

Supplementary Tables 1-2

Supplementary Figures 1-23

Table of Contents

1. Supplementary Tables

Supplementary Table 1. The recipes of precursor solutions for the synthesis.

Material	**Ionogel-60**	**Ionogel-65**	**Ionogel-70**	**Ionogel-75**	**Ionogel-80**
$VBIMBF_4$ (g)	1.20	1.30	1.40	1.50	1.60
$BMIMBF_4$ (g)	0.80	0.70	0.60	0.50	0.40
TPO-L (g)	0.012	0.013	0.014	0.015	0.016
Total (g)	2.012	2.013	2.014	2.015	2.016

The PIL/IL ionogels were fabricated by photopolymerization of 1-vinyl-3-butylimidazolium tetrafluoroborate ($VBIMBF_4$) in ionic liquid solvent 1-butyl-3-methylimidazolium tetrafluoroborate ($BMIMBF_4$) with 2,4,6-trimethylbenzoyl diphenylphosphine oxide (TPO) acting as the photoinitiator. The resulting ionogels were designated as Ionogel-xx, where "xx" denotes the overall weight percentage (wt%) of $VBIMBF_4$. In this work, ionogels with PIL contents of 60, 65, 70, 75, and 80 wt% were prepared, denoted as Ionogel-60, Ionogel-65, Ionogel-70, Ionogel-75, and Ionogel-80, respectively.

Supplementary Table 2. Characteristic peaks of FTIR spectra.

Peak position (cm^{-1})	Attribution
3135-3200	IM Ring ν(C2H)
3090-3120	IM Ring ν(CH_3)
1655	ν(C=C)
1467	IM Ring δ(CH3)
1117	IM Ring δ(C2H), δ(C4H), and δ(C5H)
1050, 1168	ν(BF_4)

In the FTIR spectrum of PIL/IL ionogels, absorption bands at 3135-3200 cm^{-1} and 3090-3120 cm^{-1} are assigned to the C-H stretching vibration of imidazolium ring. The peak at 1655 cm^{-1} is attributed to the C=C stretching vibration of ionic liquid monomer ($VBIMBF_4$). The C-H bending vibration of imidazolium group appears at 1467 and 1117 cm^{-1}. The peaks at 1050 and 1168 cm^{-1} are due to the B-F stretching.

2. Supplementary Figures

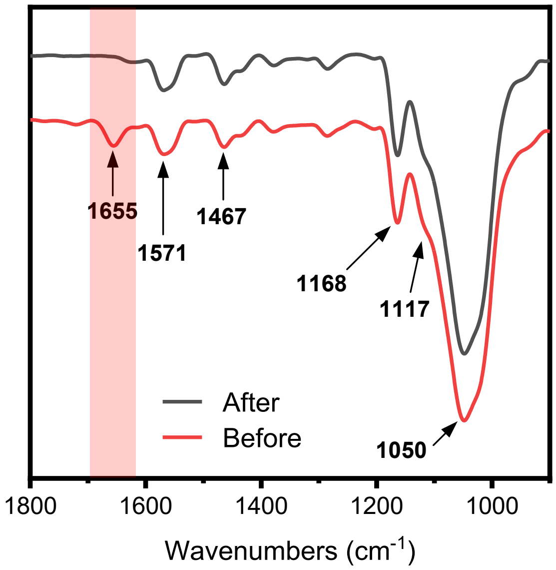

Supplementary Fig. 1 Monomer removal. FT-IR spectra comparing the PIL/IL ionogel and its precursor (before and after polymerization) in the wavenumber range of 1800–900 cm^{-1}. These data were acquired on an FTIR spectroscopy (Spectrum 100, PerkinElmer, USA) using attenuated total reflectance (ATR) mode at room temperature. The characteristic peak at 1655 cm^{-1} is attributed to C=C stretching vibration. The disappearance of this peak after polymerization indicates the absence of residual monomer.

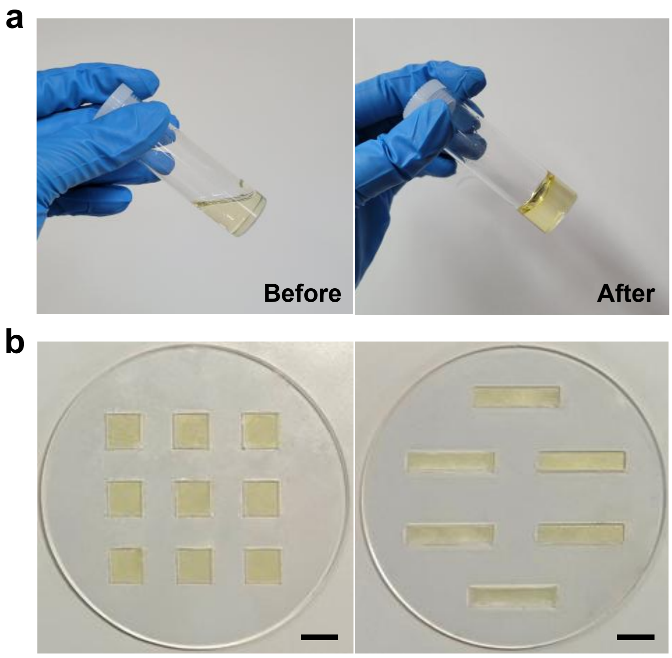

Supplementary Fig. 2 Miscibility of PIL/IL system. a Pictures of the precursor solution before and after curing. The homogeneous polymerization process can be traced without optical assistance by evaluating the transparency and viscosity of the solution. **b** Photograph of a typical PIL/IL ionogel shaped with a customized PMMA mold (scale bar, 10 mm). The poly($VBIMBF_4$) has good miscibility with $BMIMBF_4$, indicating a subtle balance of interactions between the PIL and IL.

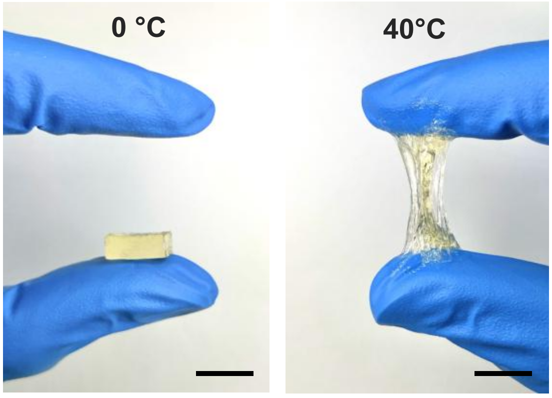

Supplementary Fig. 3 Temperature switchable ability of PIL/IL ionogel. Photographs of Ionogel-75 at different temperature. The sample temperature was pre-adjusted by heating on a hot plate or cooling on a thermoelectric plate. Scale bar, 10 mm.

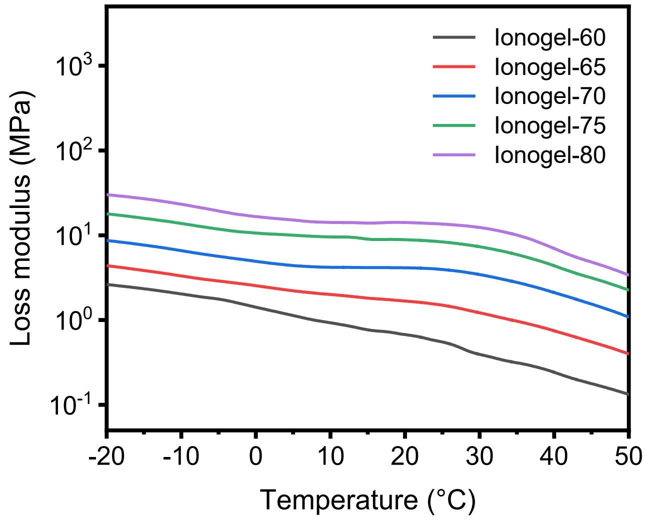

Supplementary Fig. 4 Loss modulus (E'') curves. Loss modulus versus temperature for PIL/IL ionogels with varying PIL content was shown. The loss modulus (E'') of the ionogels exhibited a moderate decline as the temperature increased from -20 to 50 °C. The increase of PIL contents significantly increased the modulus of the ionogels.

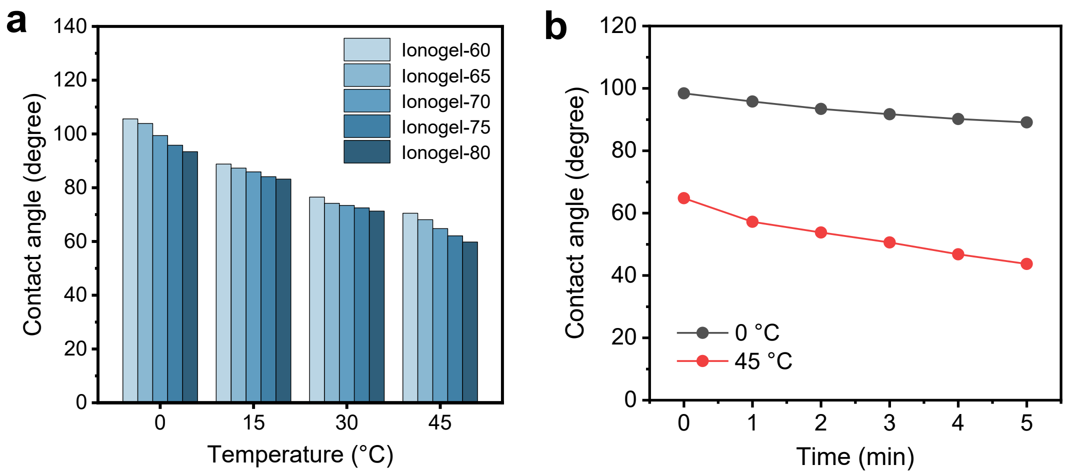

Supplementary Fig. 5 Hydrophobicity of ionogel surfaces. a Detailed contact angle measurement results of ionogel samples with various PIL contents under different temperatures. **b** Relationship between contact angle and time for Ionogel-70 at different temperatures. The contact angle is smaller at higher temperature (i.e., 45 °C) because of the enhanced surface hydrophilicity caused by the increased exposure of imidazolium functional groups. Also, water droplet spreads faster on the ionogel surface at higher temperature due to the same reason.

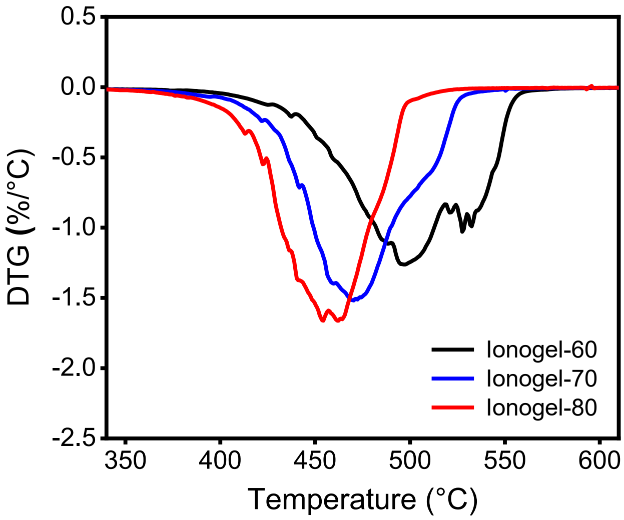

Supplementary Fig. 6 Derivative thermogravimetry (DTG) curves for different PIL contents. The decomposition onset temperature (T_o), maximum mass loss rate (DTG_{max}), and maximum mass loss temperature (T_{max}) were selected as references to evaluate thermal stability. T_o and T_{max} continued to decline as the PIL content increased. Also, DTG_{max} increased with the PIL content, indicating that thermal stability declined as the PIL content increased.

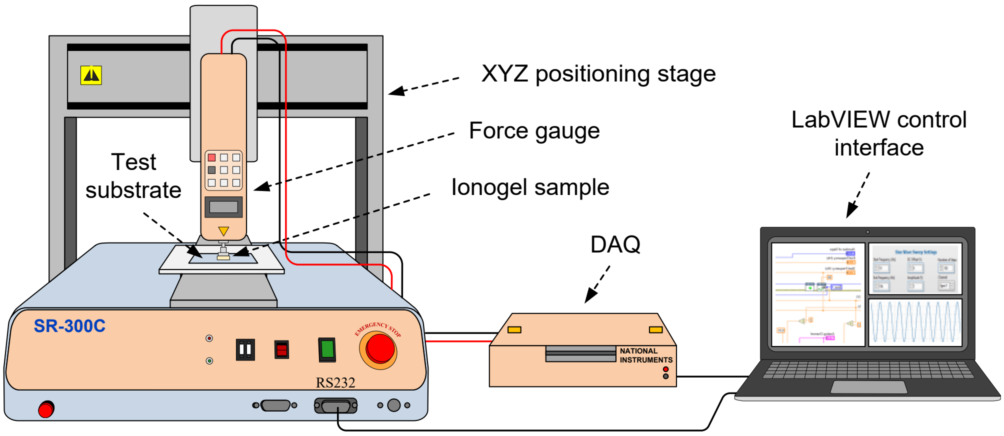

Supplementary Fig. 7 Experimental setup for adhesion measurement. The adhesion test employs an automated XYZ positioning stage (SR-300C, LTE, Taiwan) equipped with a digital force gauge (HF-1, Algol, Taiwan). The output signal of the force gauge was acquired by a data acquisition system (DAQ) and recorded via a LabVIEW-based interface. The motion of the positioning stage during the adhesion tests was also controlled by the interface. This testing setup was used for pull-off, lap-shear, and peeling tests.

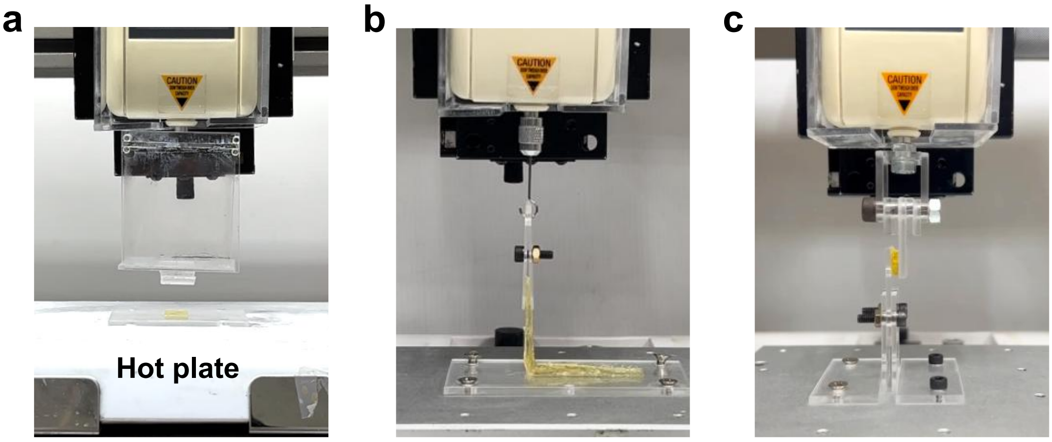

Supplementary Fig. 8 Closer views of adhesion measurement. Closer views of the samples for the adhesion measurement of **a** pull-off test, **b** peeling test, **c** lap-shear test.

a

b

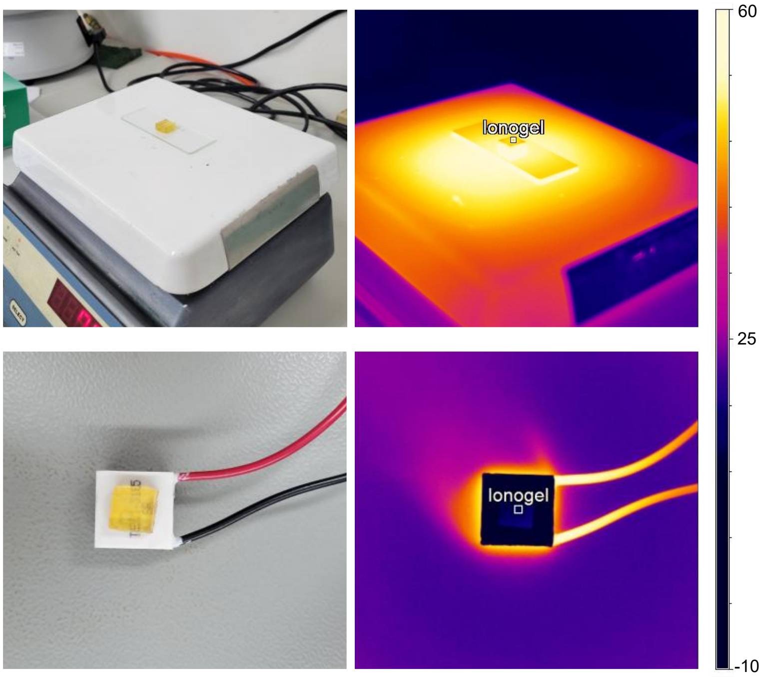

Supplementary Fig. 9 Physical images and the corresponding infrared thermal imaging photos when cooling and heating a PIL/IL ionogel sample. During the adhesion measurement, the ionogel sample was **a** heated to 40 °C using a hot plate, and **b** cooled to 0 °C using a thermoelectric cooling plate. Temperature was confirmed by an infrared camera (PI 640i, Optris GmbH, Berlin, Germany).

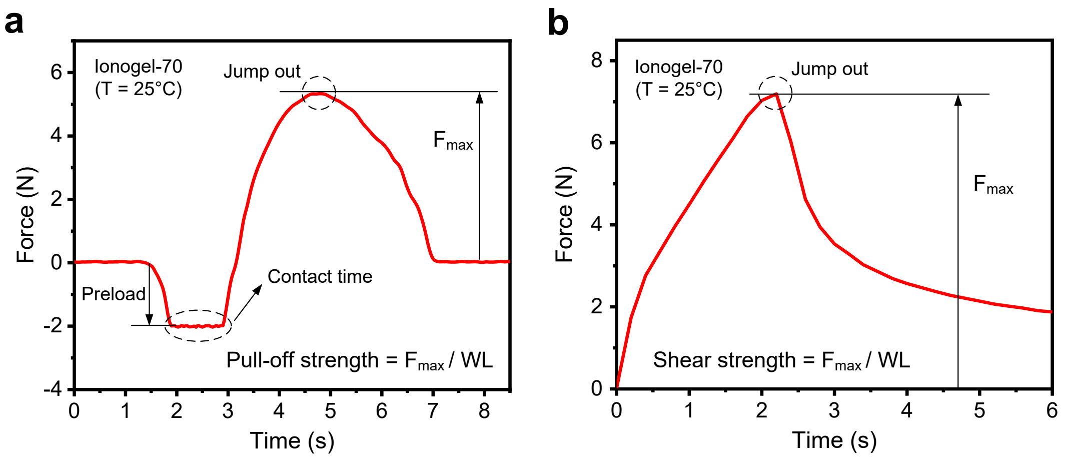

Supplementary Fig. 10 Force-Time curves from adhesion tests. a Measurement of pull-off strength. When the test substrate touched the ionogel, it would apply a preload force and stop growing when it reached 2N load. After 1s, the test substrate was lifted. The adhesion strength was defined as the maximum interfacial adhesion value at which interface debonding occurs (the point of Jump out). **b** Measurement of shear strength. The measurement was performed at a constant speed of 50 mm min^{-1}. The pull-off strength and shear strength were calculated as the maximum forces divided by the bonded area. F_{max}, the maximum force in the pull-off and lap-shear test; L, length; W, width.

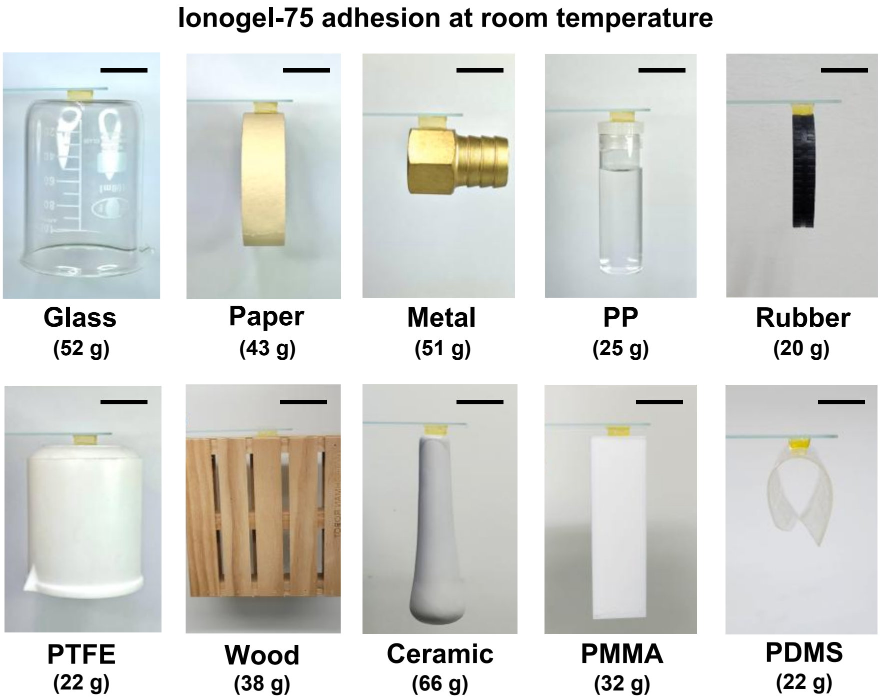

Supplementary Fig. 11 Photographs of the PIL/IL ionogel with excellent adhesion to various representative substrates. The top side of Ionogel-75 is adhered to a glass slide, and the other side is adhered to the surfaces of various materials. Then, the glass slide lifted each sample with the ionogel, and remained firmly holding the sample for more than 1 hour without any obvious peeling gaps. The results indicated that the as-prepared ionogel had excellent adhesion properties for various substrates. Scale bar, 20 mm.

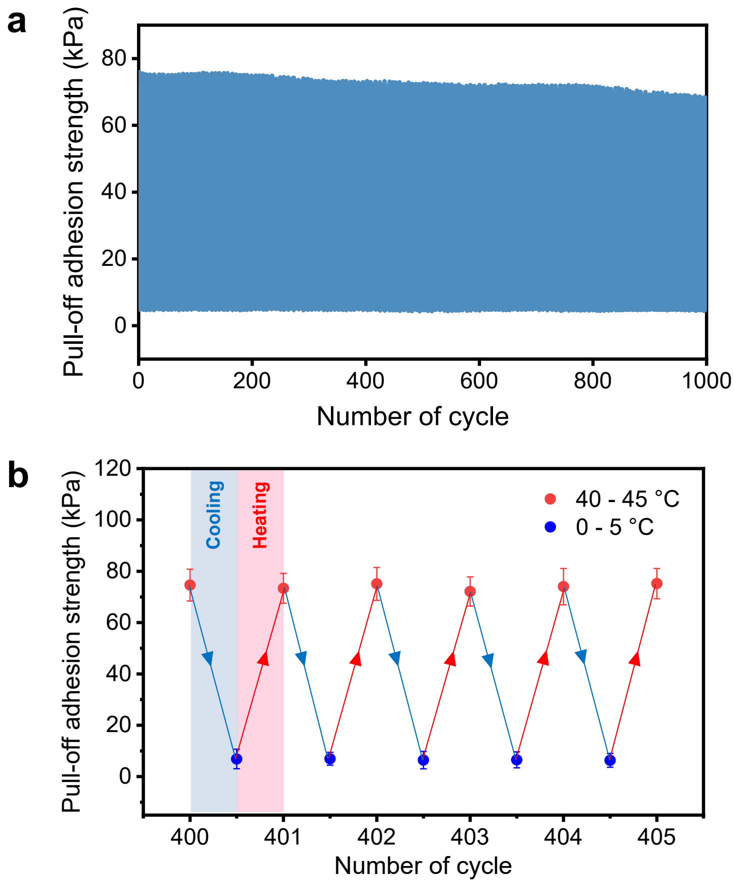

Supplementary Fig. 12 Cycle stability of switchable adhesion of PIL/IL ionogel. a The switchable adhesion cycles of ionogel-75 at high temperature (40~45 °C) and low temperature (0~5 °C) for 1000 cycles. The results demonstrated a 10.8% decrease in the pull-off strength of adhesive bonds after 1000 cycles. **b** Magnified view of cycles 400-405 from **a**. In order to control the temperature, a thermoelectric plate was used to heat or cool the ionogel sample, so that the adhesion strength at different temperatures can be tested. During the cyclic tests, the adhesion strength of the ionogel was repeatedly measured at 40 °C and 0 °C. In each cycle, the ionogel sample was heated to 40 °C and held at that temperature for 30 s prior to measurement. Subsequently, it was cooled to 0 °C, held for another 30 s, and measured again. After each heating–cooling cycle, the thermoelectric plate was switched off for 30 s to allow sufficient heat dissipation before the next cycle. The applied voltages and operating times of the thermoelectric plate during both heating and cooling processes were set to ensure that the sample temperature reliably stayed in the target temperature ranges (i.e., 40~45 °C and 0~5 °C) prior to each pull-off test. A glass plate was used as the test substrate. Error bars represent the standard deviation from at least three replicates.

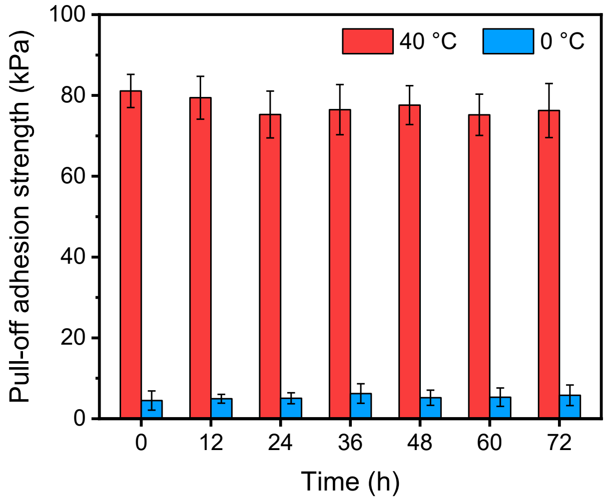

Supplementary Fig. 13 Long-term adhesion stability of PIL/IL ionogels. Under ambient room-temperature conditions, the adhesion performance of Ionogel-75 remained stable during the 3-day adhesion test without any significant decline**.** The pull-off strength of each sample was measured every 12 h at both 40 °C and 0 °C. A glass plate was used as the test substrate. Error bars represent the standard deviation from at least three replicates.

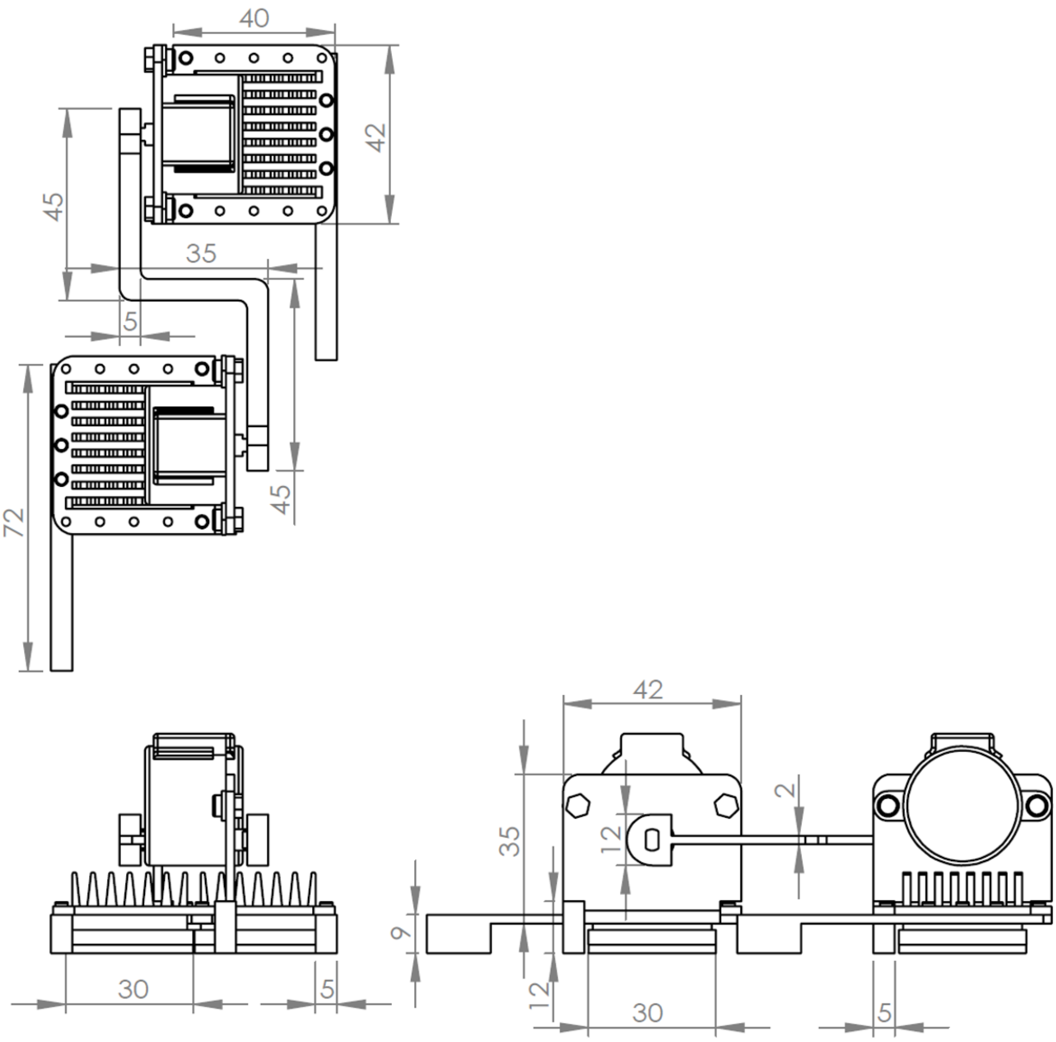

Supplementary Fig. 14 Three-view drawing of the two-foot climbing robot (Robot A). The weight of the climbing robot is about 145 g. The robot has a length of 15 cm, and its main body consists of an acrylic motor mounting frame, a footpad holder, a double-L linkage, and a rear heel. Each footpad is assembled with an ionogel adhesion module, which consists of an ionogel pad, a thermoelectric plate (TEP), and a heat sink. The thermoelectric plate (thickness, 4 mm), which is sandwiched between the ionogel pad and the heat sink, is employed to heat or cool the ionogel pad. The sizes of the ionogel pad were about 30 mm by 30 mm by 2 mm. A stepping motor (28BYJ-48, Centenary Materials Co.), which is mounted on the acrylic motor mounting frame, is employed to drive the footpad.

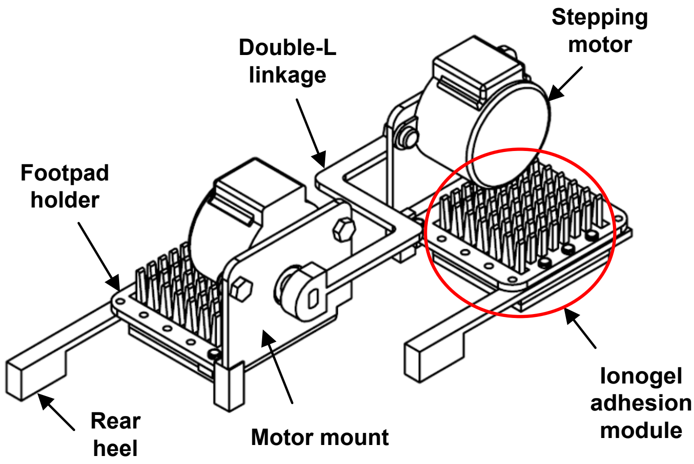

Supplementary Fig. 15 Isometric drawing of the two-foot climbing robot (Robot A).

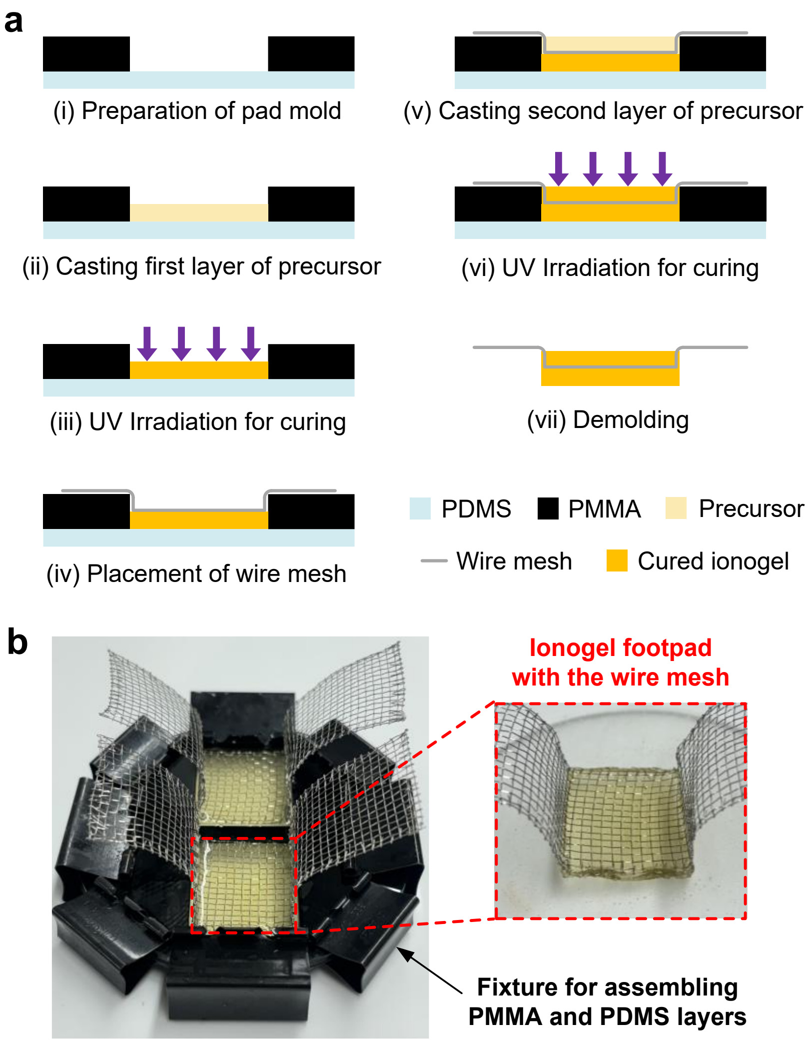

Supplementary Fig. 16 Integration of ionogel pads with metal meshes. a Fabrication process of the ionogel pad integrated with a wire mesh. **b** Pictures of cured ionogel pad integrated with the wire mesh. To facilitate the assembling process of a footpad, we developed a strategy that enables the embedding of a metal wire mesh within the ionogel. A PDMS layer served as the bottom handling substrate. An acrylic frame, fabricated by laser cutting, was clamped onto the PDMS layer to define the mold for the ionogel pad. The ionogel precursor solution was poured into the mold (half-filled). After curing under 365 nm UV light for 24 h, a wire mesh was placed on top of the cured ionogel. Then, additional precursor solution was poured into the mold (full-filled), and cured with UV light for another 24 h. After demolding, an ionogel footpad with the wire mesh was obtained.

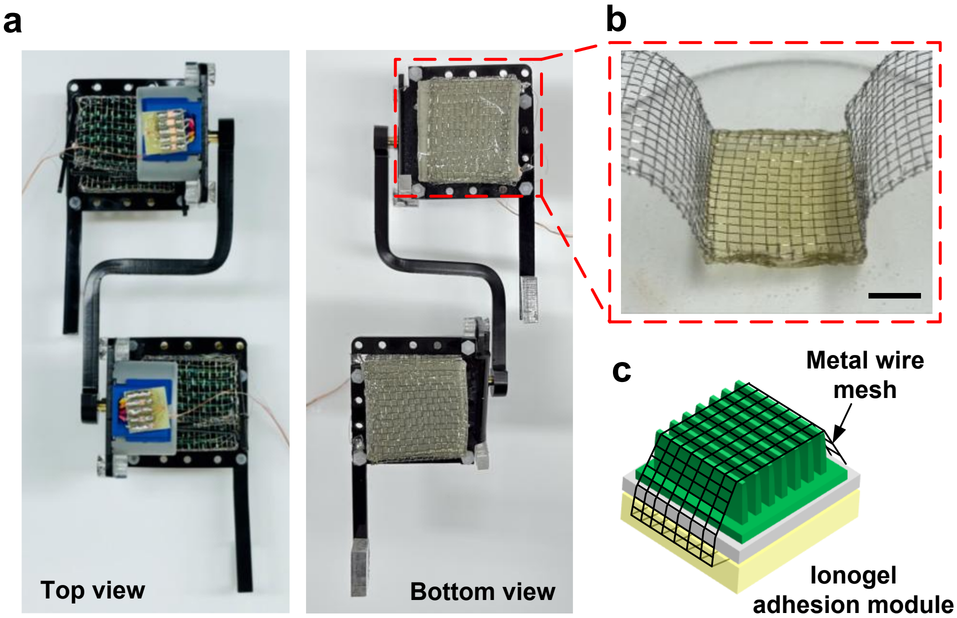

Supplementary Fig. 17 Assembly of the two-foot climbing robot. a Photographs of the two-foot climbing robot equipped with an ionogel pad. **b** The fabricated ionogel pad embedded with a wire mesh. Scale bar, 1 cm. **c** Structure of the ionogel adhesion module. The metal wire mesh was used to secure the thermoelectric plate and the heat sink, allowing them to be integrated and packaged into a single pad.

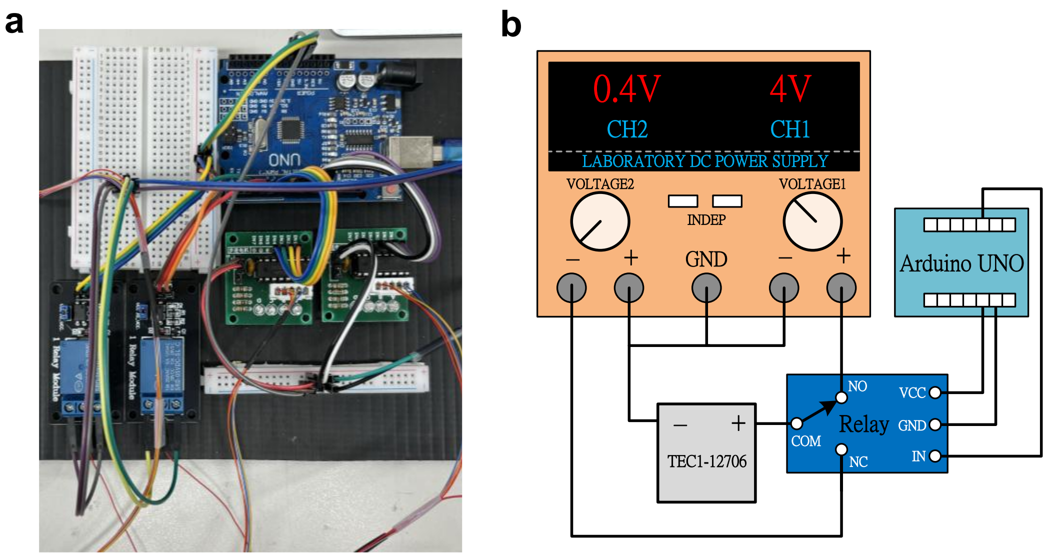

Supplementary Fig. 18 Control circuits of climbing robot. a The whole circuit for climbing robot. The circuits of each thermoelectric plate and motor were independently controlled via copper wires connected to the power supply. **b** Schematic diagram of the thermoelectric heating/cooling control circuit for a TEP module. The thermoelectric plate was driven via a relay controlled by an Arduino microcontroller board, which provided control signals to switch the applied voltage between −0.4 and 4.0 V. A positive voltage (4 V) means that the thermoelectric plate was cooling the ionogel pad; a small negative voltage (-0.4 V) means that the thermoelectric plate was mildly heating the ionogel pad.

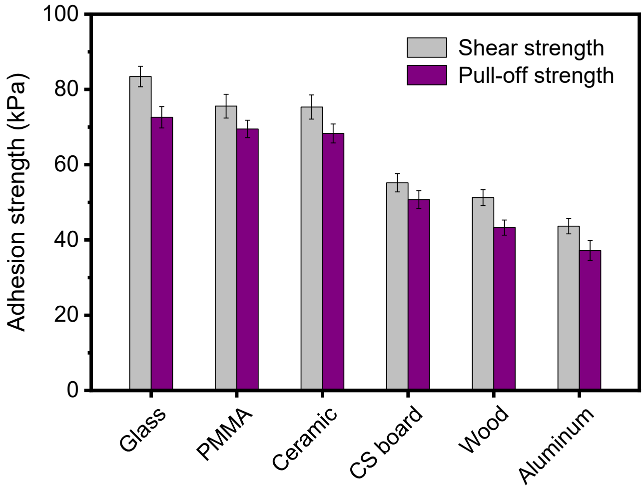

Supplementary Fig. 19 Comparison of shear and pull-off adhesion strengths on various substrates. The pull-off strength and shear strength were calculated as the maximum forces divided by the bonded area. The results show that the adhesion forces (scaled with footpad area) significantly exceed the self-weight of the two-foot climbing robot (145g). Therefore, the adhesive performance is sufficient to allow reliable climbing on both vertical and inverted surfaces.

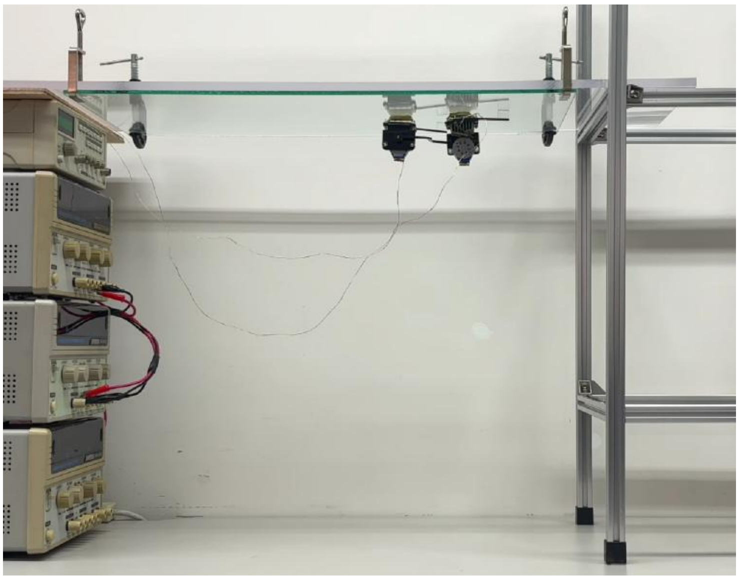

Supplementary Fig. 20 Photograph of the setup for inverted climbing. The experimental setup for testing the robot's inverted climbing on a glass surface.

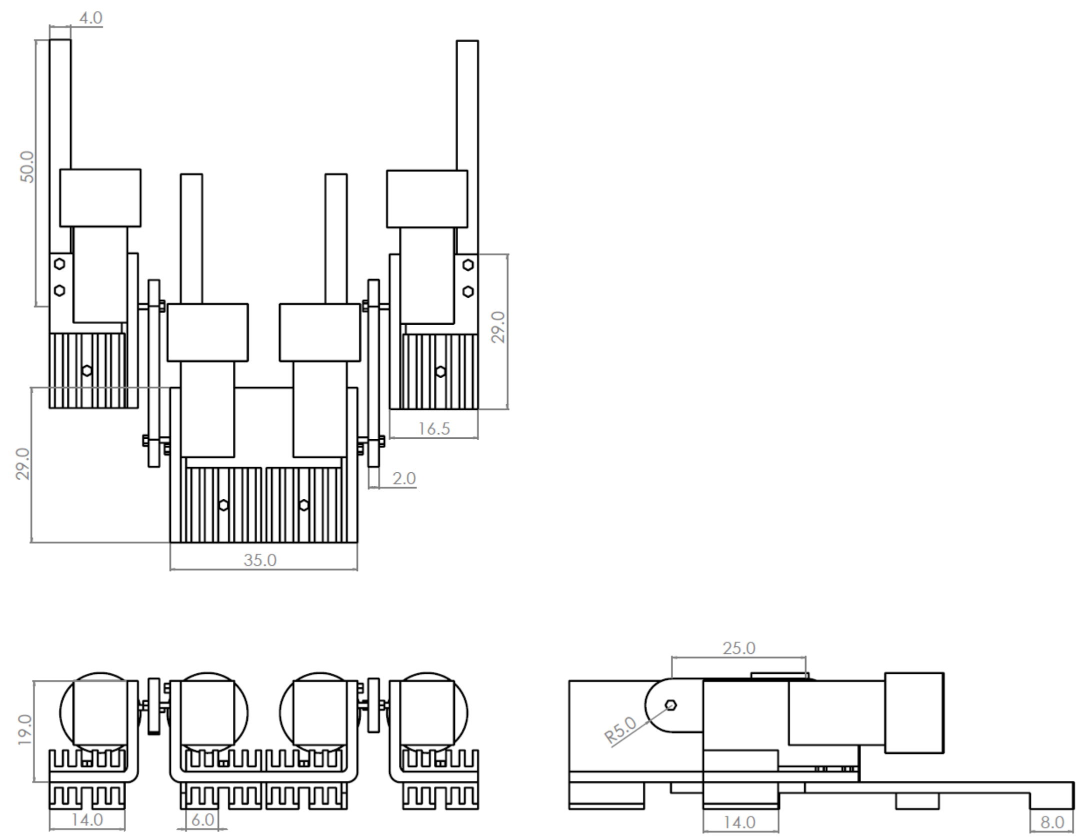

Supplementary Fig. 21 Three-view drawing of the three-foot climbing robot (Robot B). The three-foot climbing robot is mainly composed of acrylic structural components, including a central footpad, two side footpads, two linkages, and four rear heel components. The length of the robot is less than 10 cm. Four geared stepper motors (CHF-GW12T-15BY) are employed to drive the footpads. Each side footpad consists of a motor mount, a stepper motor, a rear heel, and an ionogel adhesion module. The central footpad consists of a motor mount, two stepper motors, two rear heels, and two ionogel adhesion modules. Each ionogel adhesion module comprises a thermoelectric plate (thickness, 4 mm), a top heat sink, a bottom heat sink, and an ionogel pad (14 mm by 14 mm by 3 mm). The thermoelectric plate is sandwiched between the two heat sinks. The top heat sink is the critical element for the thermoelectric plate to achieve efficient heat exchange. The bottom heat sink is primarily used to firmly incorporate an ionogel pad which provides the adhesion required for wall climbing.

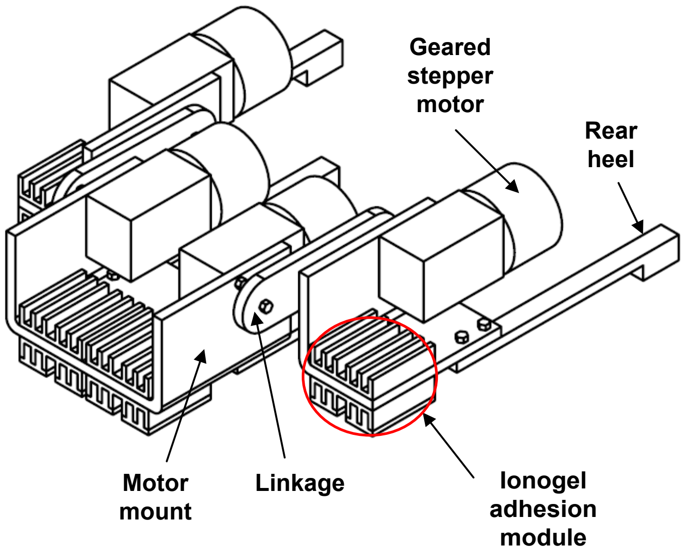

Supplementary Fig. 22 Isometric drawing of the three-foot climbing robot (Robot B).

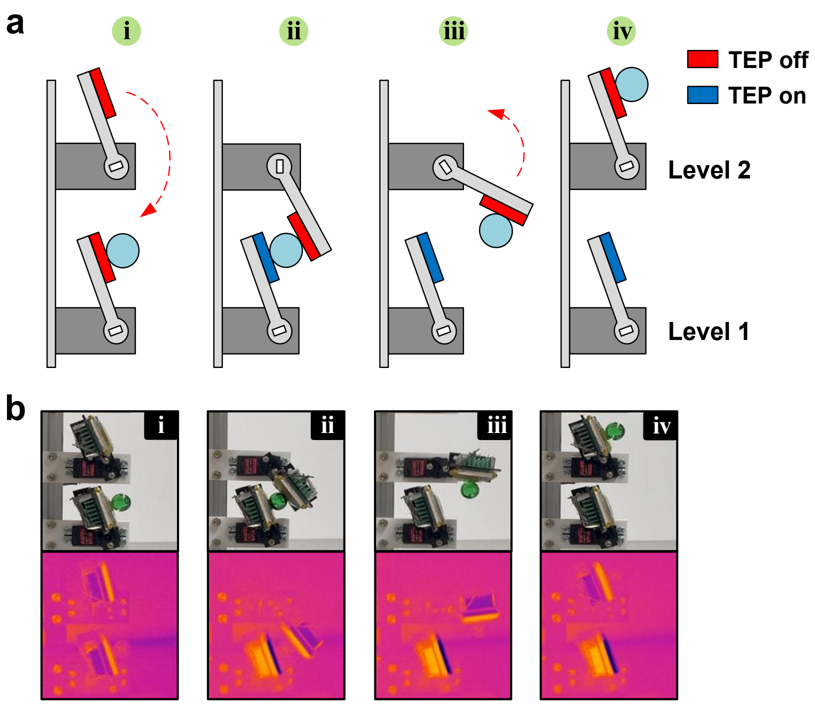

Supplementary Fig. 23 Principle of a vertical transport system. a Schematic of the transporting principle and **b** the associated snapshots of a transporting cycle in both visible and infrared images. Fig. 19a illustrates the steps of a single upward delivery process, which moves a marble from level 1 to level 2. Before the beginning of the process, the adhesion module of Level 1 is heated by its TEP, and the marble is attached to the fetch-pad. Then, the fetch-pad of Level 2 rotates, and its adhesion module, which is also heated by its TEP, touches and adheres to the marble (Fig. 23a-i). Instantly, the TEP of Level 1 cools down its adhesion module (Fig. 23a-ii). When the temperature of the ionogel of Level 1 decreases to approximately 0 °C, its adhesion strength is markedly reduced, causing the marble to detach from the fetch-pad at level 1 and be successfully transferred to level 2 (Fig. 23a-iii). Finally, the fetch-pad at level 2 returns to its initial position with the marble, ready for the transport process to next upper level (Fig. 23a-iv). Note that each TEP serves as a heater by supplying a reverse bias of 0.4V, and serves as a cooler by supplying a forward bias of 4 V.